

9.2 A Scalable 0.1-to-1.7GHz Spatio-Spectral-Filtering 4-Element MIMO Receiver Array with Spatial Notch Suppression Enabling Digital Beamforming

Linxiao Zhang¹, Arun Natarajan², Harish Krishnaswamy¹

¹Columbia University, New York, NY,

²Oregon State University, Corvallis, OR

Multiple-antenna receivers offer numerous advantages over single-antenna receivers, including sensitivity improvement, ability to reject interferers spatially and enhancement of data-rate or link reliability via MIMO. In the recent past, RF/analog phased-array receivers have been investigated [1-4]. On the other hand, digital beamforming offers far greater flexibility, including ability to form multiple simultaneous beams, ease of digital array calibration and support for MIMO. However, ADC dynamic range is challenged due to the absence of spatial interference rejection at RF/analog.

In this paper, a scalable spatio-spectral-filtering 4-element multi-in-multi-out (MIMO) receiver array is presented that combines the benefits of digital beamforming with interference rejection through RF and analog spatial notch suppression and well-established tunable RF spectral bandpass filtering. Each receiver element maintains its own I/Q baseband outputs for digitization, but incoming signals at a steerable incidence angle are rejected in each element, protecting the analog circuits from saturation and relaxing ADC dynamic range (Fig. 9.2.1). Key features include: (i) gain-boosted mixer-first receiver (GB-MF-RX) front-ends [5] that provide tunable spectral bandpass filtering and also translate an incident-angle-dependent impedance synthesized at baseband to the antenna inputs, providing spatial notch-filtering in input matching, (ii) additional baseband feedforward cancellation to further suppress the spatial notch residue, and (iii) ease of scalability through the tiling of multiple chips that have their baseband beamformed nodes connected on board. Through these techniques, a maximum of 32dB spatial rejection is achieved at the outputs. In-band output-referred IP3 (OIP3) is improved from +0dBm at the receive angles of incidence to +34dBm at the notch angle (for in-band signals, OIP3 is a more important metric as more gain makes the linearity problem more challenging). A wireless imaging demo showcases the RF/analog spatial notch suppression and digital multi-beamforming capability.

If signals from different antenna elements are connected to a common node (V_{BF} in Fig. 9.2.1 and V_{BF1-4} for differential I/Q signals in Fig. 9.2.2), then each signal will see a high impedance at that node when the signals are equal in magnitude and in phase as they arrive from the broadside direction ($\theta=0^\circ$). However, as the signals arrive from other directions, eventually reaching end-fire incidence ($\theta=\pm 90^\circ$), they will be equal in magnitude but successively 180° out-of-phase (assuming $\lambda/2$ antenna spacing in a uniform linear array), and will see an AC ground at that node. This effective “angle-pass” impedance profile can be transformed to an “angle-stop” profile through the use of a gyrator, implemented with a baseband OTA and a feedback resistor R_{FB} (Figs. 9.2.1 and 9.2.2) – at broadside, the impedance seen at each signal input ($R_{BB1,2,\dots,N}$ in Fig. 9.2.1) is low due to the high OTA gain, while at end-fire, it is simply equal to the (high) R_{FB} due to the AC ground at V_{BF} . Transparent GB-MF-RXs can translate this baseband angle-stop impedance profile to RF, providing incidence-angle-dependent input reflection coefficients that can be designed to be reflective at broadside, and matched to 50Ω at off-broadside angles. Thus, voltages from signals incident from broadside are suppressed at the antenna inputs, outputs of the RF amplifiers in the GB-MF-RXs and at the inputs of baseband OTAs. While this discussion has focused on a spatial notch at broadside, the notch can be steered in any direction by phase-shifting the LO signals of the different GB-MF-RXs relative to each other. In addition, the GB-MF-RXs provide tunable spectral filtering through C_s . Gain boosting relaxes the noise contribution of the baseband circuits as well as the passive mixer switches. Note that unlike [5], the baseband signal is sensed at the input of the OTA.

The rejection provided by this baseband spatial-notch filter (SNF) is limited to around 10dB by the finite OTA- R_{FB} loop gain, and finite switch resistance and RF amplifier gain in the GB-MF-RXs. We wish to provide large spatial suppression to challenging in-band blockers, which experience gain throughout the signal chain as spectral filtering is absent. At V_{BF} , we have formed a beam in the notch direction, thus creating a replica of blockers in that direction. This may be used for feed-forward cancellation of the residual interference in the notch direction in all elements. Variable attenuators in each element after V_{BF} scale the replica to match the residue, which is then cancelled using g_m cells identical to the g_m cells in the

main path. Phase inversion for cancellation is ensured by the inverting nature of our OTAs. Using identical g_m cells that handle equal residue and replica signals also ensures cancellation of distortion induced by the residual interference. Through the GB-MF-RXs, SNFs and these baseband feed-forward spatial-notch cancellers (FF SNCs), virtually all nodes in our receiver experience increasing levels of spatial notch suppression down the chain.

Large arrays require the tiling of multiple array RFICs. In our prototype, the formation of the beam for spatial notch suppression at baseband eases the tiling of chips, while the GB-MF-RXs translate the sharper spatial notch suppression to RF. Scalability across chips is as simple as connecting the V_{BF} node in Fig. 9.2.1 of different chips together on board. To this end, the 4 baseband beamformed nodes (V_{BF1-4}) in Fig. 9.2.2 are brought out through pads.

Based on these concepts, a 4-element prototype operating over 0.1 to 1.7GHz is implemented in 65nm CMOS (Figs. 9.2.2 and 9.2.7). Cartesian phase shifters are used in each LO path for notch steering. Figure 9.2.3 shows the measured spatio-spectral conversion gain of element 2 of the 4-element receiver array. The LO frequency is set to 500MHz and the 4 elements are assumed to be excited by a uniform linear array with $\lambda/2$ spacing at 500MHz. The 4-element receiver array shows a maximum of 32dB rejection in a steerable notch direction at in-band frequencies with both the SNF and FF SNC enabled, of which 8dB comes from the feedback-based SNF. Including the effect of the spectral filtering, a blocker in the notch direction experiences no less than 19dB rejection at all frequencies with both the SNF and FF SNC enabled. Two RFICs are tiled on board and the measured spatial notch suppression at in-band frequencies exhibits the expected sharper profile of an 8-element linear array. With the measured S-parameters across the 4 input ports, the in-band input reflection coefficient of the first element for simultaneous excitations at varying incidence angles is synthesized in Fig. 9.2.4 to show the reflection in the notch direction. IIP3/OIP3 are also shown in Fig. 9.2.4 for two-tone signals with varying angle of incidence and spectral location. The combination of the SNF and FF SNC improves the in-band OIP3 from +0dBm outside the notch angle to +34dBm at the notch angle. While the greatest benefits of spatial notch filtering are seen in-band, the out-of-band IIP3 also shows improvement from +11dBm outside the notch angle to +18dBm at the notch angle. The equivalent single-element double-sideband noise figure (NF_{DSB}) ranges from 1.7 to 4.5dB with both the SNF and FF SNC disabled. Enabling the SNF leads to 2-to-2.7dB equivalent single-element NF_{DSB} , while enabling the SNC mildly increases the noise figure to 2.2 to 4.6dB. In a wireless imaging demo (Fig. 9.2.5), the receiver array is interfaced with a 2×2 antenna array and irradiated with a weak desired signal in the presence of a spatially-distinct in-band 20dB-stronger blocker. 25 simultaneous beams in a 5×5 array are formed digitally in MatLab, with 30° coverage in each direction. An image is constructed using beam received signal strength for pixel brightness. Without analog spatial rejection (SNF and FF SNC), the receiver array outputs show clipping due to the strong blocker. The desired signal cannot be detected on the image. With the SNF and FF SNC, receiver saturation is prevented, the blocker is no longer visible and the desired weaker signal is clearly detected.

Figure 9.2.6 compares the prototype to the state of the art. In addition to the new functionality of multiple outputs for digital beamforming with spatial notch suppression, this work demonstrates very high in-band OIP3 after spatial suppression through the successive SNF and FF SNC. In addition, this work exhibits high out-of-band IIP3 and low NF_{DSB} .

Acknowledgment:

This work was sponsored by the DARPA ACT program.

References:

- [1] M. C. M. Soer et al., “A 1.0-to-4.0GHz 65nm CMOS four-element beamforming receiver using a switched-capacitor vector modulator with approximate sine weighting via charge redistribution,” in *ISSCC Dig. Tech. Papers*, pp. 64-66, Feb. 2011.
- [2] S. K. Garakoui et al., “A 1-to-2.5GHz phased-array IC based on gm-RC all-pass time-delay cells,” *ISSCC Dig. Tech. Papers*, pp. 80-82, Feb. 2012.
- [3] A. Ghaffari et al., “Simultaneous Spatial and Frequency Domain Filtering at the Antenna Inputs Achieving up to +10dBm Out-of-Band/Beam P1dB,” *ISSCC Dig. Tech. Papers*, pp. 84-85, Feb. 2013.
- [4] M. C. M. Soer et al., “A 1.0-to-2.5GHz beamforming receiver with constant- G_m vector modulator consuming < 9mW per antenna element in 65nm CMOS,” *ISSCC Dig. Tech. Papers*, pp. 66-67, Feb. 2014.
- [5] Z. Lin et al., “A 0.028mm² 11mW single-mixing blocker-tolerant receiver with double-RF N-path filtering, S11 centering, +13dBm OB-IIP3 and 1.5-to-2.9dB NF,” *ISSCC Dig. Tech. Papers*, pp. 1-3, Feb. 2015.

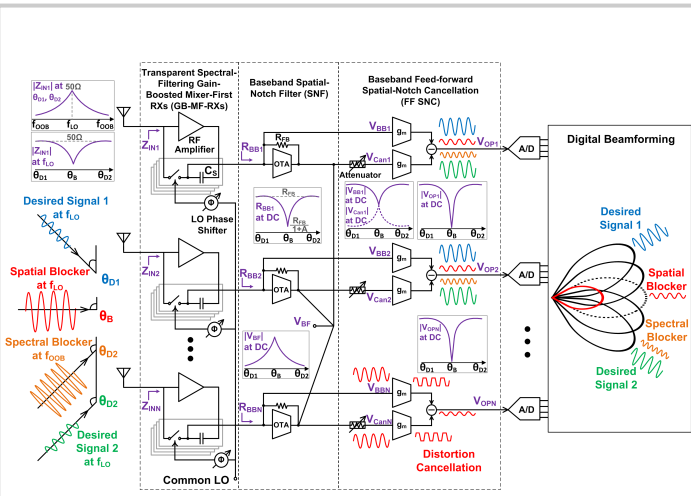


Figure 9.2.1: Scalable spatio-spectral-filtering MIMO RX array with spatial notch suppression enabling digital beamforming.

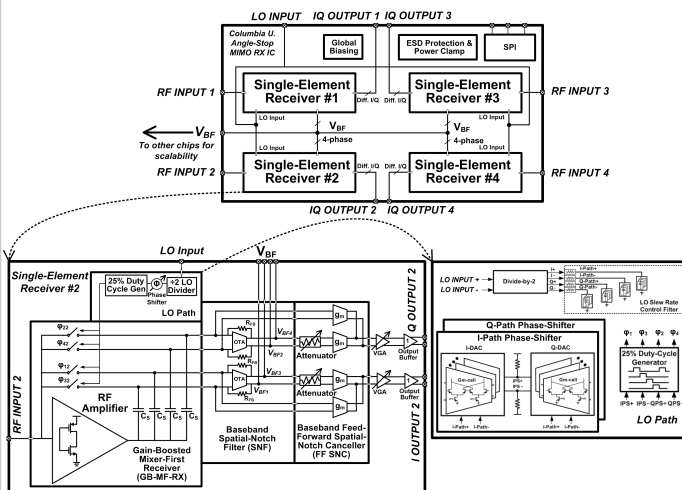


Figure 9.2.2: Block diagram of the scalable 4-element MIMO RX array.

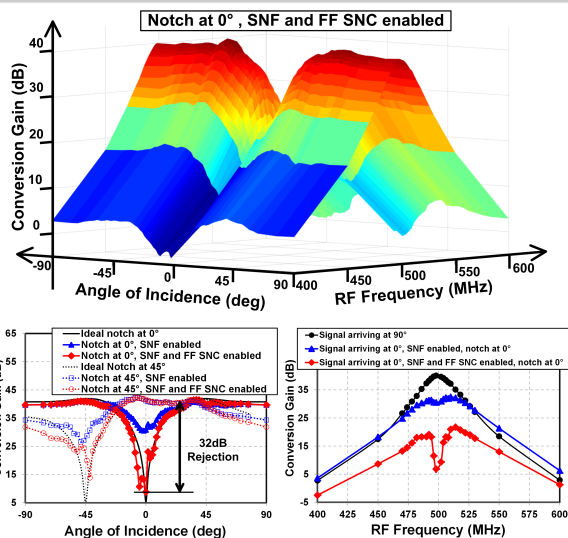


Figure 9.2.3: Spatio-spectral responses of the implemented MIMO RX array (element 2).

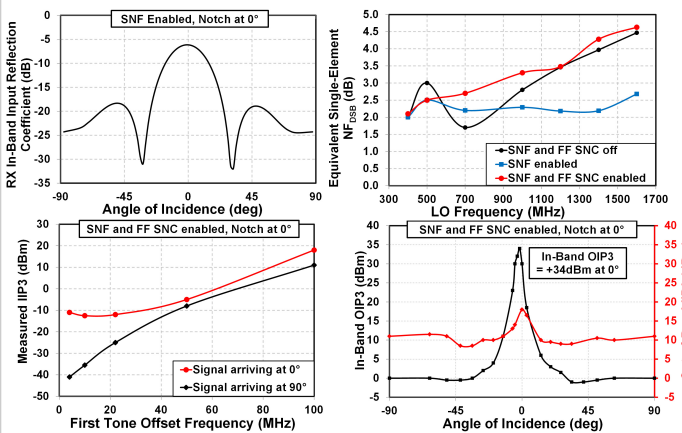


Figure 9.2.4: Measured input reflection coefficient, NF and two-tone linearity across frequency and angle of incidence.

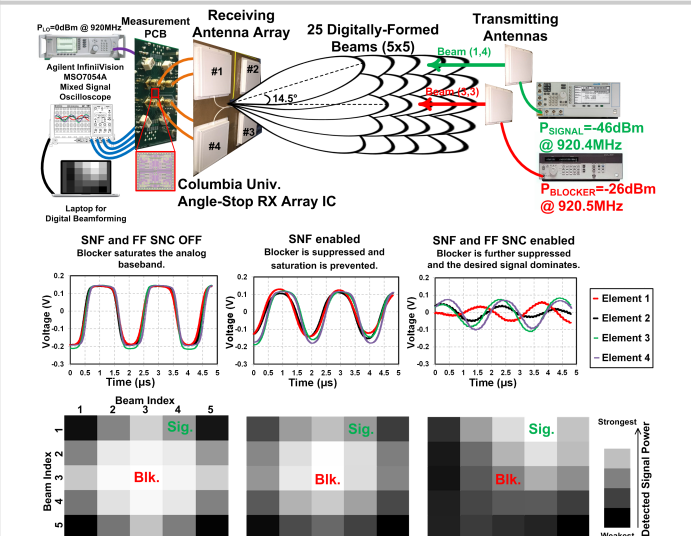


Figure 9.2.5: Wireless imaging demonstration exploiting digital multi-beamforming with analog / RF spatial notch suppression.

	JSSC,2010 [6]	ISSCC,2011 [1]	ISSCC,2012 [2]	ISSCC,2013 [3]	ISSCC,2014 [4]	This Work
Architecture	Phase Oversampling Beamforming Downconverter based Phased Array	Baseband Switched-Cap. Vector Modulator based Phased Array	Gm-C All-Pass RF True-Time-Delay-based Phased-Array	Spatio-Spectral Phased Array with Angle-Pass Filtering at Antenna	Baseband-Combined Constant-Gm Vector Modulator based Phased Array	Scalable Spatio-Spectral MIMO array with Spatial Notch Rejection
CMOS Process	90nm	65nm	140nm	65nm	65nm	65nm
Chip Area (mm ²)	1.92	1.08	1	2.25/0.97 ¹	1.06/0.2 ¹	2.25/1.69 ¹
Supply Voltage (V)	1.2	1.2	1.8	NR	1	1.2
Number of Inputs/Outputs	4/1	4/1	4/1	4/1	4/1	4/4
RF Operating Frequency Range (GHz)	4 (narrow-band)	1 - 4	1-2.5	0.6 - 3.6	1 - 2.5	0.1 - 1.7
Single-element Conversion Gain (dB)	15	16	15	-1 ²	12	41
Equivalent Single-element NF _{OSB} ³ (dB)	13	10	8-10	5-8 ³	6	1.7 - 4.5 ⁴ 2 - 2.7 ⁵ 2.2-4.6 ⁵
Phase Resolution (bits)	5	5	4.7	3	5.5	6
Spatial Suppression (dB)	>24	> 25	25	38	NR	32
In-Band OIP3 ⁶ (dBm)	+17 ¹⁰	+15 ¹⁰	+2 ¹⁰	+1 - +8 ⁸	+13 ¹⁰	0 ⁸ +34 ⁸
Out-of-Band IIP3 ⁹ (dBm)	NR	NR	NR	+20 ^{11,12}	+5 ¹¹	+11 ¹ +18 ⁸
Power Consumption (4-element, mW)	166	308@2.5GHz	450	68 - 195	26 - 36	83 (analog) 65(digital) @500MHz

Figure 9.2.6: Performance summary and comparison to the state of the art.

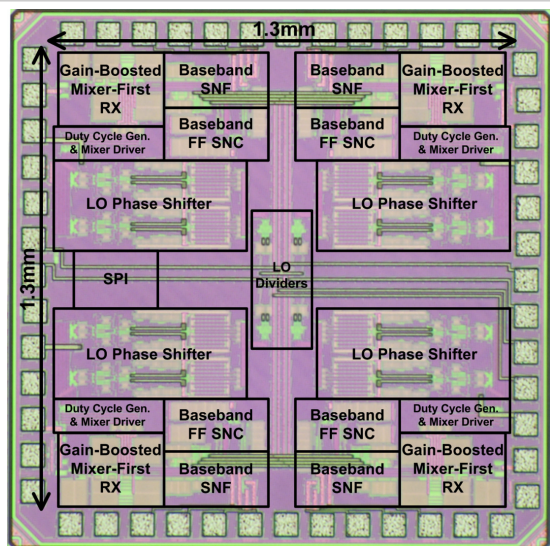


Figure 9.2.7: Die micrograph.